^{1}H-NMR study of the spin dynamics of fine superparamagnetic nanoparticles

L. Bordonali,[1,2,3] Y. Furukawa,[3] M. Kraken,[4] F. J. Litterst,[4] C. Sangregorio,[5] M. F. Casula,[6] and A. Lascialfari[2,7,8]

[1]*Department of Physics "E. Amaldi," Università Uniroma TRE, Roma, Italy*
[2]*Department of Physics "A. Volta," Università di Pavia, I-27100 Pavia, Italy*
[3]*Ames Laboratory, and Department of Physics and Astronomy, Iowa State University, Iowa 50011, USA*
[4]*Institute of Condensed Matter Physics, Technische Universität Braunschweig, D38106 Braunschweig, Germany*
[5]*CNR-ISTM Milano and INSTM, I-20133 Milano, Italy*
[6]*INSTM and Department of Chemical Sciences, Università di Cagliari, Cagliari, Italy*
[7]*Department of Molecular Sciences Applied to Biosystems, Università degli Studi di Milano, via Trentacoste 2, I-20134 Milano, Italy*
[8]*S3-CNR, Institute of Nanosciences, via Campi 213/A, I-41125 Modena, Italy*

We report a broadband ^{1}H-NMR study of the temperature spin dynamics of nearly monodisperse dextran-coated γ-Fe$_2$O$_3$ magnetic nanoparticles. We observed a maximum in $T_1^{-1}(T)$ that decreases in amplitude and shifts toward higher temperatures with increasing field. We suggest that this is related to the progressive superparamagnetic spin blocking of the ferrite core. The data can be explained by assuming a single electronic spin-spin correlation time and introducing a field-dependent distribution of anisotropy energy barriers.

I. INTRODUCTION

Over the last 30 years a substantial number of studies concerning the magnetic properties of superparamagnetic (SPM) nanostructures have been published, an effort motivated by the interest in the fundamental physics of low-dimensional magnetic systems and a widespread impact on medical and technological applications.[1] However, the issue of broad polydispersity has hampered the advances in this field for a long time and only recently it has been possible to synthesize SPM nanoparticles with a sufficiently narrow volume distribution,[2] thus enabling more detailed studies of the physical mechanisms regulating the single particle as well as the collective magnetic behavior. The magnetism of SPM ferrite nanoparticles is usually modeled by Néel's model, which describes, in single domain particles, a spin-blocking process controlled by the magnetic anisotropy energy barrier, although more complicated and refined models have been developed to overcome its limitations. A crucial issue not taken into account by Néel's model is the different spin dynamics of the uncompensated surface spins with respect to the core ones.[3,4] Moreover, magnetic interparticle interactions of dipolar character, always present to some extent in a powder sample, give rise to complex behavior when coupled with surface effects.

Techniques such as Mössbauer spectroscopy and electron magnetic resonance spectroscopy have been successfully employed to gain insights into the spin dynamics of ferrite nanoparticles.[3,5–7] On the other hand, no attempt has been made so far to explore the local spin dynamics on a broad temperature range by NMR techniques, the actual papers in the literature being limited to NMR spectra of nuclei belonging to magnetic ions showing low-temperature spin freezing.[8] NMR has already been successfully employed for the study of the magnetic properties of molecular iron clusters, such as Fe$_6$,[9] Fe$_8$,[10,11] Fe$_{10}$,[12] and Fe$_{30}$,[13] where an enhancement in $1/T_1$ at temperatures of 10–30 K revealed dynamics driven by the coupling of the paramagnetic ions with acoustic phonons.[14] The same intent is shared by the investigation of very small iron-based nanoparticles, taking

the NMR research on iron complexes a step further on the scale of the spin-systems dimensions.

In this paper we present an attempt to address the problem of the spin dynamics of fine magnetic nanoparticles (MNPs) by measuring the ^{1}H-NMR spectra and longitudinal and transverse relaxation rates on dry powders of dextran-coated γ-Fe$_2$O$_3$ (maghemite) nanoparticles. Our investigation was made possible by the magnetic coupling of the hydrogen nuclei of the polymer shell surrounding the particles with the iron spins of the ferrite core via dipolar and eventually contact hyperfine interaction with protons of oxydriles at the surface of the ferrite core. Thus, even though the probing nuclei do not sense single local spins of the ferrite core, the mechanisms behind the dynamical behavior of the nanoparticle magnetization can be accessed. It should be also pointed out that the presence of the organic shell conveniently allows to rule out the presence of sizable additional interactions such as Ruderman-Kittel-Kasuya-Yoshida (RKKY) superexchange or interfacial exchange couplings that would lead to a more complex scenario.

Findings from the NMR investigation are supported by a comparison with the results of ^{57}Fe Mössbauer spectroscopy experiments, also reported in this paper.

II. SYNTHESIS OF γ-Fe$_2$O$_3$ PARTICLES

The synthesis of the iron oxide nanocrystals was performed by coprecipitation under alkaline conditions of Fe(II) and Fe(III) (Ref. 15) in the presence of dextran. An amount of 5.5 g of dextran (Leuconostoc mesenteroides, average molecular weight 9.000–11.000 g mol^{-1}) was dissolved in 2 ml of distilled water. Then 1 ml of a 2M solution of iron(II) chloride tetrahydrate (FeCl$_2 \cdot$ 4H$_2$O, $\geqslant$99%) in deionized and degassed water and 4 ml of a 1M iron(III) chloride hexahydrate (FeCl$_3 \cdot$ 6H$_2$O, 97%) solution were deoxygenated by purging with nitrogen for 30 min at room temperature and were then added to the dextran solution under stirring. Then 50 ml of a freshly prepared 1M NH$_3$ (28–30 %) solution was then added dropwise over 30 min into the mixture at room temperature under magnetic stirring. A color change from brown to black
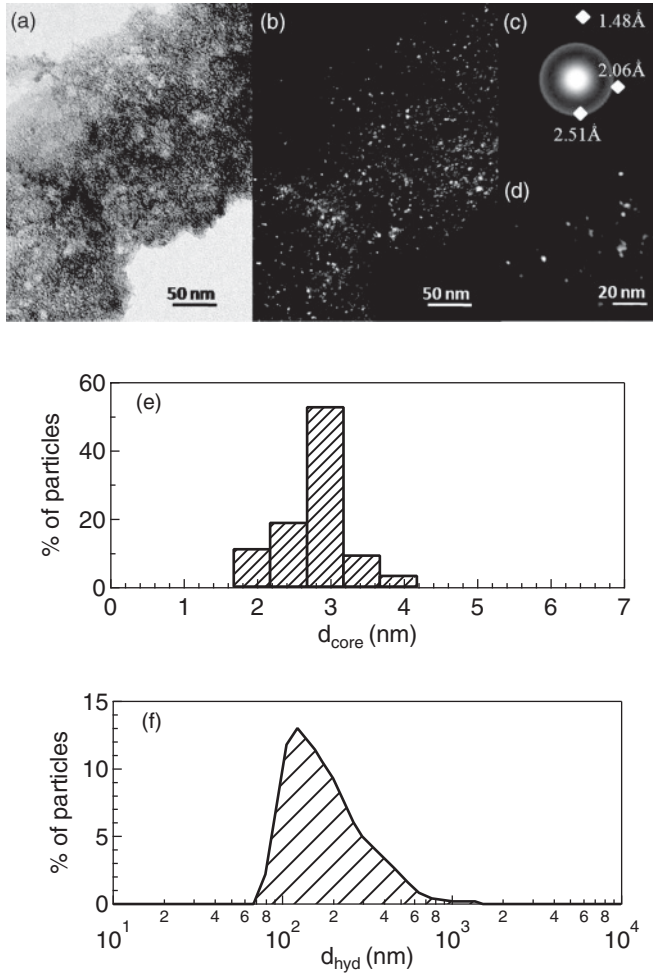
FIG. 1. Transmission electron microscopy images of the dextran–iron oxide sample under (a) bright field and (b) dark field modes and (c) the corresponding selected area diffraction; (d) close-up dark field view of the sample. The two graphs at the bottom display (e) the magnetic core diameter and (f) the hydrodynamic diameter distributions.

was observed in the reaction mixture during the addition of ammonia solution. The dextran amount with respect to the overall reaction volume is 10% wt/vol, and the resultant mixture was stirred for a further hour to promote particle growth. The final pH was recorded to be around 9.5. The particles were then purified from unbound polymer by three cycles of washing and magnetic collection and finally dried at 60 °C for 2 days. Figure 1 displays the TEM images of the dextran-coated γ-Fe$_2$O$_3$ sample and the measured size dispersion. The core diameter and hydrodynamic diameter distributions of the prepared material were investigated by means of TEM and dynamic light scattering (DLS) measurements. We found an average ferrite core diameter of 3.0 ± 0.5 nm and an average hydrodynamic diameter of 122 ± 11 nm (polydispersity index 0.4).

III. MEASUREMENTS OF AC AND DC MAGNETIC SUSCEPTIBILITY

Magnetic data were obtained by ac and dc magnetic susceptibility measurements, performed on a MPMS-XL7 Quantum Design superconducting quantum interference
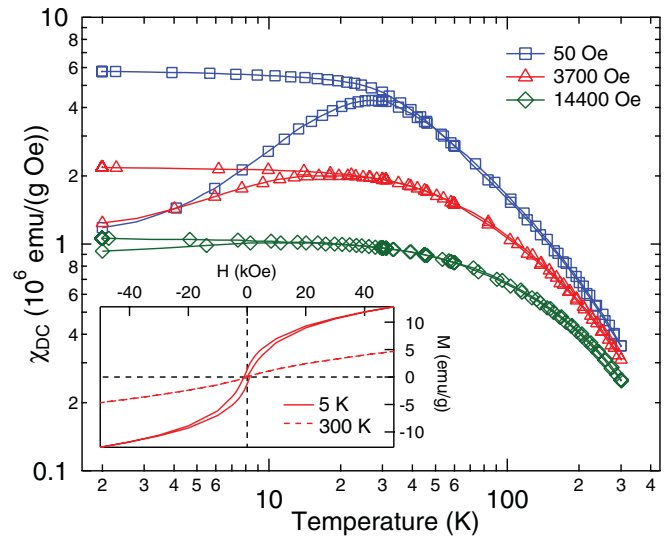

FIG. 2. (Color online) The dc susceptibility FC/ZFC curves vs T at three different fields. An irreversibility temperature is definable for all three data sets. Inset: Hysteresis cycle at $T = 5$ K and $T = 300$ K.

device (SQUID) magnetometer in the temperature range 2–300 K and applied fields $H = 50$ Oe, 3.7 kOe, 6.8 kOe, and 14.4 kOe. For ac measurements the amplitude of the ac field was $H_{ac} = 3$ Oe and investigated frequencies were $\nu_{ac} = 1, 4, 16, 63, 250,$ and 1000 Hz in zero and applied dc fields. Hysteresis loops were recorded in the $H = [-50 \text{ kOe}, +50 \text{ kOe}]$ field range at $T = 5, 300$ K.

Figure 2 shows zero field cooled (ZFC) and field cooled (FC) magnetization curves measured at 50 Oe, 3.7 kOe, and 14.4 kOe between 2 and 300 K. The departure of the ZFC/FC magnetization curves and the peak in the ZFC curve are characteristics of SPM nanoparticles, the peak marking the so-called blocking temperature T_B. It is remarkable that a blocking temperature can be found even for very high applied fields (14.4 kOe), as confirmed by the surviving cusp in the ZFC magnetization curve. The position of the maximum decreases with increasing field, as it would be expected.[16] The corresponding magnetization loop at 5 K is shown in the inset of Fig. 2: the magnetization does not reach a saturation value either at room temperature or at 5 K and it stands well below the value 80 emu/g, the saturation magnetization in bulk maghemite. It is commonly accepted that in a core-shell framework and high fields irreversibility is the signature for the presence of disorder due to canted surface spins.[17–20] To investigate the behavior of the anisotropy energy barrier at high applied fields and to gain better insight into the field dependency of the barrier distribution, we measured the ac susceptibility curves in applied magnetic dc fields $0 \leqslant H_{dc} \leqslant 1T$. Remarkably, an average barrier Δ can be extracted by ac measurements at all fields by fitting the plot of the relaxation time τ as a function of temperature with an Arrhenius function $[\tau(T) = 2\pi/\nu(T) = \tau_0 \exp(\Delta/T)]$. The values of τ were obtained from the maximum of χ'' using the relation $\omega\tau = 1$, ω being the working frequency. The parameters Δ and τ_0 extracted from ac data are (Δ, τ_0) = (630.12 K, 1.499×10^{-18} s/rad), (183.92 K, $8.445 \times$

10^{-13} s/rad), (66.29, 2.766×10^{-7} s/rad), respectively, for $H = 0$ Oe, 3.7 kOe, and 6.8 kOe. Since τ_0 usually assumes values in the range 10^{-9}–10^{-12} s for noninteracting superparamagnets in zero applied field, our results imply that Néel's model breaks down and that the activation energy is temperature dependent, a partly expected result on the basis of the imbalance of the two wells of the energy-level diagram when a magnetic field is applied. Unphysical τ_0 values are commonly encountered when magnetic nanoparticles are coupled by dipolar interactions (see Ref. 21 and references therein). The rather large values for Δ also reflect the presence of such couplings.

In this respect, the formation of a spin-glass-like state was previously proposed to account for the dynamics observed by the ac technique in ferromagnetic and ferrimagnetic nanoparticle systems of varying sizes; in some cases the freezing to a superspin-glass state has been related to strong interparticle interactions. The interpretation of such dynamics, however, is rather difficult, since the onset of a spin-glass-like state could be labeled as either a cooperative effect between the SPM superspin of each ferrite nanoparticle or a consequence of the magnetic frustration between the iron spins at the surface layer of each particle, following from the uncompensated chemical bonds and lattice symmetry breaking. In very small particles, such as those studied in this paper, it seems plausible that a disordered magnetic state covering the whole particle could be found at low temperatures. On the other hand, as pointed out in Ref. 17, the high field irreversibility, witnessed by an unsaturated hysteresis cycle, rules out this hypothesis in favor of a different scenario that sees the core and surface regions as very distinct from one another, the disordered region being limited to the surface layer only.

To test the hypothesis of interparticle interactions leading to a spin-glass-like state, we followed a procedure already applied to γ-Fe_2O_3 nanoparticles,[22] fitting the ac data at zero applied static field to the critical slowing-down law:

$$\tau = \tau_0[T_g(\omega)/T_g - 1]^{-z\nu}, \qquad (1)$$

where $z\nu$ is the product of the dynamical critical exponent z and the critical exponent ν associated with the correlation length. No temperature dependence of the attempt time τ_0 has been considered in the investigated temperature range. $T_g(\omega)$ has been extracted by $\chi'(T)$ as the temperature of the curve maximum at each working frequency ω (see Fig. 3(a) and inset). T_g has been fixed to the temperature of the maximum in the ZFC curve at $H = 50$ Oe, $T_g = T_B = 25.5$ K. We found $\tau_0 = 1.22 \pm 0.62 \times 10^{-10}$ s/rad and $z\nu = 10.2 \pm 0.3$; the value for the exponent $z\nu$ is in excellent agreement with values expected for the three-dimensional Ising-like spin glasses ($10 < z\nu < 12$) and with other results for maghemite nanoparticles (Parker *et al.*[22]: $z\nu = 10.3 \pm 0.3$, $d = 9$ nm; Leite *et al.*[23]: $z\nu = 8.0 \pm 0.2$, $d = 3$ nm). Still, the ambiguity between a "collective" superspin-glass state and a "single-particle" spin-glass-like state remains since, although using a critical slowing-down model is qualitatively correct, this method fits either case.

Regarding the NMR investigation presented here, it is worth noticing that a superspin-glass state is easily destroyed after the application of a moderate magnetic field;[24] thus, any dynamic
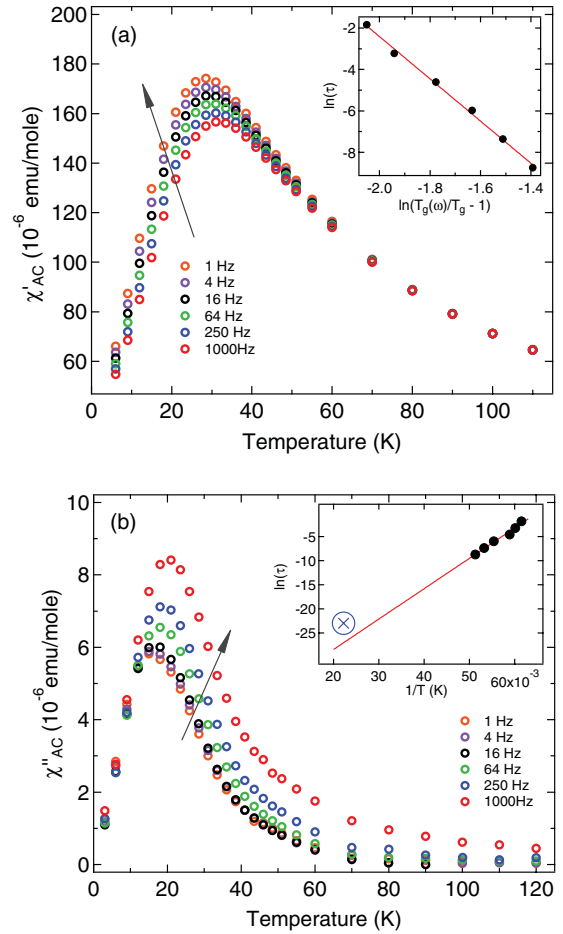

FIG. 3. (Color online) Temperature dependence of the (a) in-phase and (b) out-of-phase components, $\chi'(T)$ and $\chi''(T)$, of the magnetic susceptibility at different excitation frequencies. The arrows indicate increasing frequencies. Inset of (a): log-log plot of τ vs $T_g(\omega)/T_g - 1$ for the dextran-capped γ-Fe_2O_3 nanoparticles and fit to the dynamic slowing-down power law. Inset of (b): Arrhenius plot extracted from ac χ'' susceptibility at zero field and fit. The data point from Mössbauer experiments is included and indicated with a circled cross symbol (refer to Sec. IV in this paper).

contribution that would be generated by the internal field fluctuations associated with the onset of a "collective" glassy state at low applied static fields can be safely neglected at fields greater than $\sim 10^2$ Oe. We conclude that under the relatively intense fields of a NMR experiment ($H_0 > 10^3$ Oe) the aforementioned ambiguity is removed and no superspin-glass state can be found; hence, it is only possible to probe the superparamagnetic thermal activation of the inner shell of the γ-Fe_2O_3 core and, eventually, the effects of a faster dynamics of the disordered surface layer.

In a perfectly monodisperse sample with negligible interparticle interactions, one expects that the anisotropy energy barrier would disappear if a high magnetic field was applied; however, the presence of a disordered surface layer creates a complex multiminima energy landscape which should broaden the distribution[25] while the joint effect of the applied field and dipolar interactions shifts the average anisotropy barrier toward lower values, introducing substantial low-energy contributions.[26] An estimate of the Zeeman energy E_Z at

3.4 and 14.4 kOe yields values of the order of 10^2–10^3 erg while the particle magnetic anisotropy energy E_A as calculated from the bulk magnetocrystalline anisotropy constant $K_{bulk} = 4.7 \times 10^4$ erg/cm^3 is only of the order of 10–10^2 erg. However, it is quite common to witness a difference of two orders of magnitude[16,27,28] between the bulk anisotropy energy density and the effective anisotropy energy density in a nanoparticle with size $d \leqslant 5$ nm, because additional sources of anisotropy come into play (i.e., shape, surface, magnetostriction contributions, and the dipolar interaction contribution). Thus, it is not unusual to have $E_Z < E_A$ and a double-minima (or multiminima) energy landscape even at the high fields commonly found in solid-state NMR experiments.

As we proceed with the discussion of ^{1}H-NMR measurements we show that the hypothesis of a reduced energy barrier is consistent with the results of the analysis on the nuclear spin-lattice relaxation (NSLR) rate temperature dependence.

IV. ^{57}Fe MÖSSBAUER SPECTROSCOPY ON γ-Fe$_2$O$_3$ MNPS

^{57}Fe Mössbauer spectroscopic measurements have been performed at temperatures ranging from 4 to 300 K on an absorber with an area density corresponding to about 0.2 mg ^{57}Fe/cm^2. A conventional transmission spectrometer with sinusoidal velocity sweep was used. As source served about 12 mCi of ^{57}Co in a rhodium matrix kept at room temperature. The absorber containers were made of nylon and fixed within copper clamps. Temperature control and measurement were performed with a Lakeshore DRC-91C using a calibrated Si diode attached to the copper clamp. The absorbers were kept in a static He exchange gas atmosphere of about 0.2–0.4 mbar in a flow He cryostat (CRYOVAC). Temperature stability was better than 0.1 K.

Figure 4 shows a representative set of absorption spectra at various temperatures. Clearly visible is the gradual broadening of the magnetically split hyperfine pattern at lowest temperatures leading to a collapse to a doublet spectrum above about 50 K. This scenario is typical for relaxation spectra of very small particles. (For a recent review, see Ref. 7.) At low temperatures the fluctuation rates of particle moments are slow compared to nuclear Larmor precession of ^{57}Fe, and a magnetically split pattern may be observed. At high temperatures the fluctuations lead to motional narrowing; i.e., the time-averaged hyperfine magnetic field vanishes and only the nuclear quadrupole interaction in the local electric field gradient at the Fe site (a doublet spectrum) is observed. The collapse occurs for fluctuation rates between 10^{10} and 10^{11} s^{-1}. Due to a distribution in fluctuation frequencies caused by a distribution in particle size and anisotropy energy this is not a sharp transition but smeared over some temperature range. Typically one defines the blocking temperature at the time scale of Mössbauer spectroscopy as the temperature where about 50% of the spectral area reveals magnetic hyperfine interaction, whereas the other 50% are (super)paramagnetic. In our case this takes place around 45 K.

In Fig. 4 we have deliberately not included fits of theoretical models to the experimental data. The estimate of the blocking temperature is practically independent of the method of analysis. (We report on a detailed analysis comparing various methods for noninteracting and interacting particles,

multilevel relaxation, superferromagnetic model, etc., in a forthcoming publication.) In Fig. 3(b) we have included the blocking temperature derived from the Mössbauer data in the inset. As can be seen it is in excellent agreement with the extrapolation of the ac data.

It should be noticed that spectra recorded even at the lowest temperatures still reveal a strong temperature-independent line broadening. This is in contrast to spectra found from other small particles of ferrites, which show sharp spectra (see examples given in Ref. 7). The broadening therefore cannot be related to magnetic dynamics. We interpret it with inhomogeneous magnetic distributions of hyperfine fields due to the shell structure of the particles having strongly canted spins.

V. ^{1}H-NMR EXPERIMENTS ON γ-Fe$_2$O$_3$ MNPS AND DISCUSSION

^{1}H-NMR proton NSLR rates T_1^{-1} and spectra were measured using a standard pulsed NMR spectrometer in the temperature range [1.5 K, 120 K] at $H = 3.7$ kOe, 14.4 kOe. The ^{1}H NMR signal at $T > 120$ K was very low and thus it was not possible to collect data in a reasonable acquisition time. The recovery curves of the nuclear magnetization have been collected by integrating the spin-echo signal following a sequence of saturating radio frequency pulses (90°-180°/90°-90° sequences). All ^{1}H-NMR spectra have been measured point by point by integrating the echo signal while sweeping the external field around the central field position $H_L = \omega_L/\gamma_P$, where γ_P is the proton gyromagnetic ratio and ω_L is the fixed proton Larmor frequency.
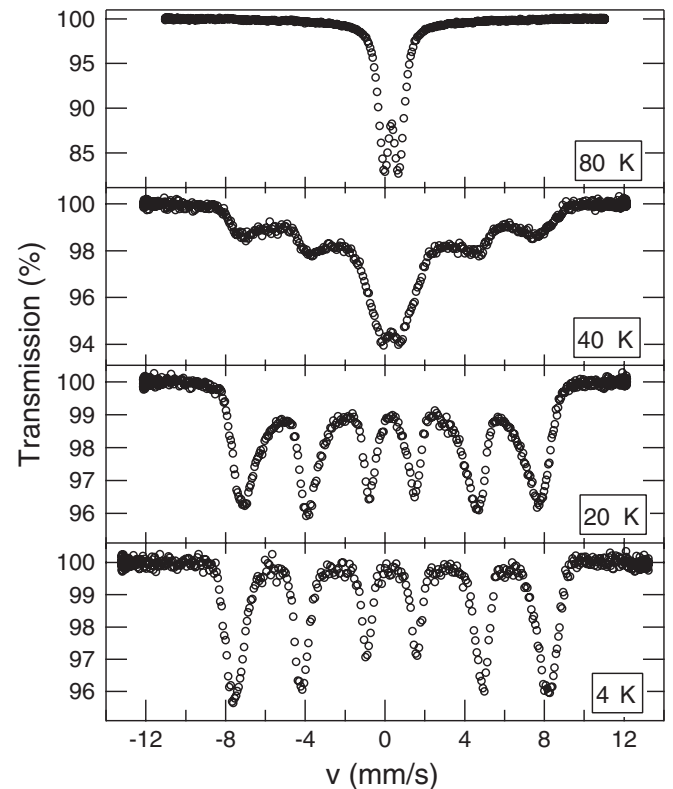

FIG. 4. Collection of zero zero-field Mössbauer spectra recorded for the γ-Fe$_2$O$_3$ sample at various temperatures.
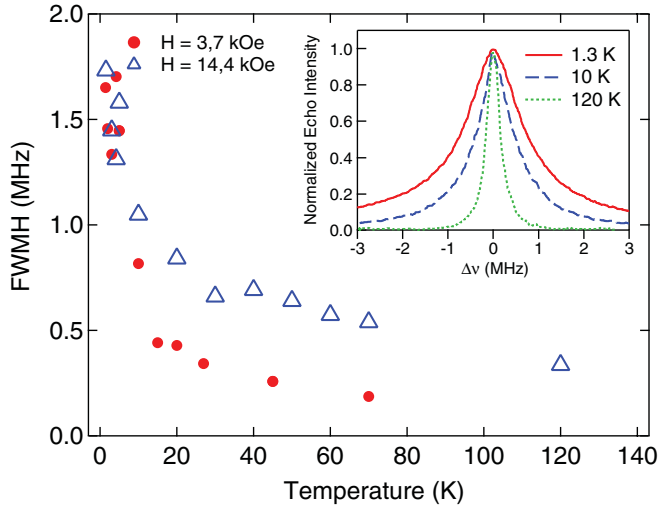
FIG. 5. (Color online) Temperature dependence of the proton NMR spectrum linewidths collected at temperatures above 1.5 K with evidence for a superparamagnetic spin blocking. The inset shows a selection of measured spectra.

FIG. 6. (Color online) Average proton spin-lattice relaxation rate (T_1^{-1}) plotted vs temperature for two external magnetic fields. Inset: semilog plot of the distributions of energy barriers related to the two investigated static fields, as extracted from Eq. (2).

The ¹H-NMR line shapes for $T = 1.3$, 10, and 120 K at $H = 3.7$ kOe are reported in the inset of Fig. 5; for the sake of simplicity we did not report the spectra at 14.4 kOe. All spectra have a Lorentzian symmetric line shape from which the full width at half maximum (FWHM) was calculated and plotted in Fig. 5 against the measuring temperature. The temperature dependence of the NMR linewidth is ascribed to an inhomogeneous component, i.e., a distribution of hyperfine dipolar fields at the nuclear proton sites due to interaction of protons with the Fe magnetic moments. It should be also noted that (i) the protons closer to the surface, responsible for the probing of the surface layer dynamics, are experiencing a distribution of dipolar fields due to the disordered magnetic configuration of the electronic spins in the layer, and (ii) the spectra are intrinsically broadened because of inequivalent proton sites (i.e., different Larmor frequencies) in the dextran coating. A distribution from orientational disorder of powders must also be taken into account. At both fields the linewidth progressively increases with decreasing temperature, from 0.2–0.6 MHz at ~70 K to ~1.5 MHz at ~1.5 K, following the progressive freezing of local spins. Under $T = 4$ K the NMR linewidth saturates, marking the achievement of a completely blocked state of the SPM moments.

The recovery of the longitudinal nuclear magnetization was found to be nonexponential at both applied static fields $H = 3.7$ kOe, 14.4 kOe. The deviation from the monoexponential behavior can be related to a distribution of relaxation rates due to the presence of inequivalent proton sites and an orientational distribution in the powders. Therefore, in order to measure a consistent relaxation parameter, an effective T_1 reflecting the fastest relaxing nuclei, defined as the time at which the nuclear magnetization has recovered 40% of the equilibrium value, was taken into account.

Figure 6 reports the values of T_1^{-1} as a function of temperature for two different applied static fields. Our main result is the observation of a maximum in $T_1^{-1}(T)$ at $T \sim 45$ K
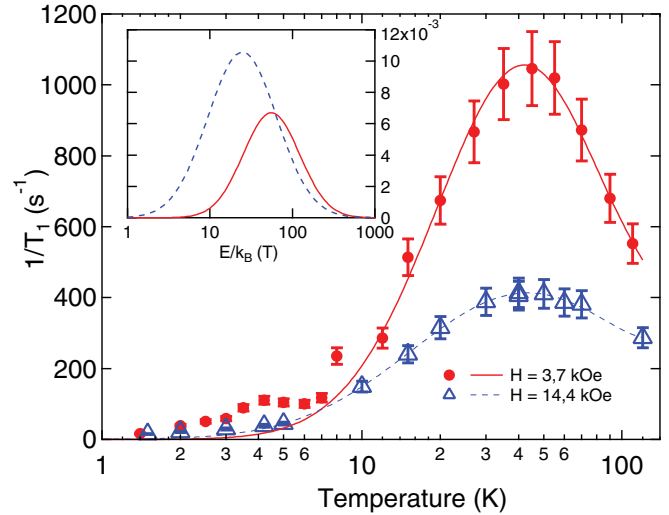
for both applied static fields. An additional shoulder is also visible around 4 K on the curve collected at $H = 3.7$ kOe.

In order to give an interpretation of the spin dynamics behind the behavior in $T_1^{-1}(T)$ we assumed a simple Bloembergen Purcell Pound (BPP)-like spectral density function,[29] which can be obtained from the original Moriya theory of nuclear relaxation in paramagnets,[30,31] of the form $J(\omega, T) = A(T)\chi(T)T\tau_c(T)/[1 + \omega^2\tau_c^2(T)]$, where $\tau_c(T)$ is the temperature-dependent electronic spin-spin correlation time. The prefactor $A\chi(T)T$ represents the mean square value of the local hyperfine field fluctuations and contains the temperature dependence of the static magnetic susceptibility $\chi(T)$. Assuming that the correlation time $\tau_c(T)$ is the one governing the relaxation of the magnetization of the internal SPM core, we have taken into account that for SPM nanoparticles a "simplified" Arrhenius law is obeyed: $\tau_c(T) = \tau_0 \exp(\Delta/T)$. Although the choice of a standard thermally activated dynamics model is controversial when interparticle interactions are not negligible, the heuristic model employed to explain the NMR data is greatly simplified assuming to a first approximation an Arrhenius-like law instead of a more appropriate expression, e.g., a Vogel-Fulcher law, which would still be considered a phenomenological solution but becomes senseless when T approaches the critical temperature T_C.

Despite the good monodispersity of our sample, as previously discussed, the application of an external magnetic field and the existence of a disordered surface layer give rise to a distribution of energy barriers. For this reason in the expression of T_1^{-1} we assumed a lognormal distribution $P(E)$ of energy barriers E, with median value $\bar{E}$ and scale parameter σ_E. In doing so, we guarantee that the energy barrier distribution can be related to a volume distribution modified by the surface effect, also allowing for lower energy contributions. The heuristic formula employed to fit the NSLR data is

$$\frac{1}{T_1}(T) = A\chi(T)T \int_0^\infty P(E) \frac{\tau_c(T,E)}{1 + \omega_L^2 \tau_c^2(T,E)} dE, \quad (2)$$

TABLE I. Collection of dc and NMR key parameters obtained from the fitting of the experimental data (see text).

dc	$H_{c,5\,K}$	$T_{B,50\,Oe}$	$T_{B,3.7\,kOe}$	$T_{B,14.4\,kOe}$
Parameters	-1020 Oe	25,5 K	18.9 K	12.5 K
NMR	$\tau_{0,3.7\,kOe}$	$\tau_{0,1.44\,T}$	$E_{3.7\,kOe}$	$E_{14.4\,kOe}$
Parameters	8.35×10^{-11} s	2.60×10^{-11} s	58.24 K	23.88 K

where

$$P(E) = \frac{1}{E \sigma_E \sqrt{2\pi}} \exp\left(-\frac{[\ln E - \ln(\bar{E})]^2}{2\sigma_E^2}\right),$$

$$\tau_c(T,E) = \tau_0 \exp(-E/T).$$

The integration in Eq. (2) was performed numerically during the fitting procedure. The NSLR data were fitted to Eq. (2) and the resulting curves are reported in Fig. 6. The fit yields energy barrier distributions peaked at $E_{peak}/k_B = 58.2$ K for $H = 3.7$ kOe and $E_{peak}/k_B = 23.8$ K for $H = 14.4$ kOe and parameters $\sigma_E = 0.786$ and $\sigma_E = 0.963$, respectively, while the values of τ_0 extracted from the $1/T_1$ data are $\tau_0 = 8.35 \times 10^{-11}$ and 2.60×10^{-11} s/rad, respectively, in good agreement with the expected values for a typical superparamagnet. Magnetic parameters extracted by dc magnetometry and NMR measurements are collected in Table I.

We suggest that the difference between the attempt time τ_0 measured by χ_{ac} and ^{1}H-NMR is possibly due to the presence of interparticle dipolar interactions having different effects on local (detected by NMR) and bulk (revealed by χ_{ac}) spin dynamics.[31–34] The NMR probes are mostly sensing the magnetic environment at a very local level, thus being more sensitive to the single-particle superspin and to the surface layer dynamics while any cooperative effects driven by the interparticle dipolar coupling have been quenched by the high static NMR field, as discussed in Sec. III.

The inset of Fig. 6 reports the energy barrier distributions related to the fit curves in the main plot; it is clearly visible how the mean value of the distribution moves toward lower energies, as is generally expected when increasing the external static field. Under the current interpretation of the phenomenon, it should not come as a surprise that the position of the anomaly in T_1^{-1} turns out to be nearly the same for both applied fields: considering the expression of the spectral density function of Eq. (2), the higher the measurement frequency (higher fields), the higher in temperature the position of the peak should be; however, the shift toward lower energies in the distribution of energy barriers pushes the peak for $H = 14.4$ kOe ($\omega_L \simeq 61$ MHz) down in temperature, in apparent alignment with the peak for $H = 3.7$ kOe ($\omega_L \simeq 16$ MHz).

Finally, the presented heuristic model does not explain the presence of a shoulder at low temperature. This shoulder can be tentatively attributed to an enhancement due to the aforementioned increased contribution to the barriers distribution at nearly zero energy values originating from dipolar couplings between particles[26] and the application of a magnetic field. As already mentioned in Sec. IV, the temperature-independent broadening observed in Mössbauer spectra collected at $T \sim 4$ K supports the hypothesis of a highly disordered magnetic phase at the surface. Thus, alternatively, the anomaly at

$T \sim 4$ K in $T_1^{-1}(T)$ could be explained as an effect of the fluctuations of the surface spins being faster than the core spin fluctuations, yielding a freezing of surface spins at lower temperatures.[6]

The effects of both the core and surface dynamics on NMR quantities greatly depend on the coupling of Fe spins and H nuclei in the outer organic shell via transferred hyperfine interaction; however, a theoretical estimate of the values of the hyperfine coupling constant would require a density functional approach to the problem and for the case of even the smallest nanoparticles ($d \simeq 1$ nm) the feat would be quite challenging if not unfeasible. Therefore, further experimental and theoretical effort is needed at low temperatures in order to confirm the presence of the mentioned effects.

VI. CONCLUSIONS

In summary we have presented a broadband ^{1}H-NMR study of the spin dynamics of nearly monodisperse γ-Fe$_2$O$_3$ nanoparticles encapsulated in an organic shell. We report an enhancement in the proton NSLR rates $1/T_1$ at low temperatures and postulate that the observed dynamics is related to a SPM moment blocking regulated by a field-dependent distribution of anisotropy energy barriers, modified by interparticle dipolar interactions and surface effects. Data from Mössbauer spectroscopy experiments support the dynamics observed by NMR and also give hints on possible low-temperature surface phenomena. Different results between the ac susceptibility measurements and the NMR experiments have been been found and interpreted in the light of the different dynamics observed by the two nonequivalent techniques: The ac data, analyzed with a critical slowing-down law commonly applied to the study of spin-glass states in condensed matter, yielded results compatible with both a single-particle spin-glass-like state in the surface layer of the maghemite core and a collective superparamagnetic spin-glass state originating from the magnetic dipolar couplings in the nanoparticle ensemble. The latter hypothesis has been excluded from the interpretation of the NMR data on the basis of the fragility of the spin-glass-like collective state in a magnetic field in interacting magnetic particle systems.

The most promising perspective opened by our results concerns the possibility of detecting dynamical effects on magnetic nanoparticles by means of standard solid-state NMR spectroscopy and relaxometry, which have only been applied to colloidal suspensions of magnetic nanoparticles,[35,36] though in completely different frameworks. We also reasonably put forward the idea that the NMR technique is a valuable complement to Mössbauer spectroscopy on magnetic nanoparticles when properly coated with a material featuring a sensitive NMR probe.

Future experimental work should also consider the convenience of resorting to NMR for fundamental studies on the mesoscopic quantum effect in very small ($d < 2$ nm) magnetic particles,[37,38] at the boundary between classical and quantum behavior. The application of NMR to small nanoparticles may therefore give relevant contributions to the effort of filling the gap between the world of magnetic clusters ($S_{tot} < \sim 30$) and the classical world of the larger nanoparticles ($S_{tot} > \sim 100$).

[1] Q. Pankhurst, N. Thanh, and S. Jones, J. Phys. D **42**, 224001 (2009).

[2] H. Cui, Y. Feng, W. Ren, T. Zeng, H. Lv, and Y. Pan, Recent Pat. Nanotechnol. **3**, 32 (2009).

[3] G. C. Papaefthymiou, E. Devlin, A. Simopoulos, D. K. Yi, S. N. Riduan, S. S. Lee, and J. Y. Ying, Phys. Rev. B **80**, 024406 (2009).

[4] K. L. Krycka, R. A. Booth, C. R. Hogg, Y. Ijiri, J. A. Borchers, W. C. Chen, S. M. Watson, M. Laver, T. R. Gentile, L. R. Dedon, S. Harris, J. J. Rhyne, and S. A. Majetich, Phys. Rev. Lett. **104**, 207203 (2010).

[5] E. Lima Jr., A. Brandl, A. Arelaro, and G. Goya, J. Appl. Phys. **99**, 083908 (2006).

[6] R. D. Desautels, E. Skoropata, and J. van Lierop, J. Appl. Phys. **103**, 07D512 (2008).

[7] S. Mørup, M. Hansen, and C. Frandsen, in *Comprehensive Nanoscience and Technology*, edited by D. L. Andrews, G. D. Scholes, and G. P. Wiederrecht (Academic, Amsterdam, 2011), pp. 437–491.

[8] P. Panissod, *NMR of Nanosized Magnetic Systems, Ultrathin Films, and Granular Systems, in Magnetism: Molecules to Materials III: Nanosized Magnetic Materials* (Wiley-VCH Verlag GmbH, Weinheim, 2001).

[9] B. Pilawa, R. Boffinger, I. Keilhauer, R. Leppin, I. Odenwald, W. Wendl, C. Berthier, and M. Horvatić, Phys. Rev. B **71**, 184419 (2005).

[10] Y. Furukawa, K. Kumagai, A. Lascialfari, S. Aldrovandi, F. Borsa, R. Sessoli, and D. Gatteschi, Phys. Rev. B **64**, 094439 (2001).

[11] Y. Furukawa, K. Aizawa, K.-I. Kumagai, A. Lascialfari, S. Aldrovandi, F. Borsa, R. Sessoli, and D. Gatteschi, Mol. Cryst. Liq. Cryst. **379**, 191 (2003).

[12] M. Affronte, J. C. Lasjaunias, and A. Cornia, Eur. Phys. J. B **15**, 633 (2000).

[13] E. Micotti, D. Procissi, A. Lascialfari, A. Carretta, P. Kögerler, F. Borsa, M. Luban, and C. Baines, J. Magn. Magn. Mater. **272–276**, 1099 (2004).

[14] S. H. Baek, M. Luban, A. Lascialfari, E. Micotti, Y. Furukawa, F. Borsa, J. van Slageren, and A. Cornia, Phys. Rev. B **70**, 134434 (2004).

[15] R. Massart, IEEE Trans. Magn. **17**, 1247 (1981).

[16] G. F. Goya and M. P. Morales, J. Metastable Nanocryst. Mater. **20**, 673 (2004).

[17] B. Martínez, X. Obradors, L. Balcells, A. Rouanet, and C. Monty, Phys. Rev. Lett. **80**, 181 (1998).

[18] M. P. Morales, S. Veintemillas-Verdaguer, M. I. Montero, C. J. Serna, A. Roig, L. Casas, B. Martínez, and F. Sandiumenge, Chem. Mater. **11**, 3058 (1999).

[19] H. Kachkachi, A. Ezzir, M. Nogues, and E. Tronc, Eur. Phys. J. B **14**, 681 (2000).

[20] E. Tronc, D. Fiorani, M. Noguès, A. M. Testa, F. Lucari, F. D'Orazio, J. Grenèche, W. Wernsdorfer, N. Galvez, and C. Chanéac, J. Magn. Magn. Mater. **262**, 6 (2003).

[21] X. Batlle and A. Labarta, J. Phys. D **35**, R15 (2002).

[22] D. Parker, V. Dupuis, F. Ladieu, J.-P. Bouchaud, E. Dubois, R. Perzynski, and E. Vincent, Phys. Rev. B **77**, 104428 (2008).

[23] E. Leite, J. Coaquira, W. Viali, P. Sartoratto, R. Almeida, P. Morais, and S. Malik, J. Phys.: Conf. Ser. **200**, 072060 (2010).

[24] P. E. Jönsson, S. Felton, P. Svedlindh, P. Nordblad, and M. F. Hansen, Phys. Rev. B **64**, 212402 (2001).

[25] N. Pérez, P. Guardia, a. G. Roca, M. P. Morales, C. J. Serna, O. Iglesias, F. Bartolomé, L. M. García, X. Batlle, and A. Labarta, Nanotechnology **19**, 475704 (2008).

[26] O. Iglesias and A. Labarta, Phys. Rev. B **70**, 144401 (2004).

[27] G. Goya, T. Berquo, F. Fonseca, and M. Morales, J. Appl. Phys. **94**, 3520 (2003).

[28] G. Goya, S. L. Gomez, and S. M. Shibli, J. Metastable Nanocryst. Mater. **22**, 33 (2004).

[29] N. Bloembergen, E. M. Purcell, and R. V. Pound, Phys. Rev. **73**, 679 (1948).

[30] C. P. Slichter, *Principles of Magnetic Resonance*, Springer Series in Solid-State Sciences (Springer Verlag, NY, 1996).

[31] T. Moriya, Prog. Theor. Phys. **16**, 23 (1956).

[32] A. H. Morrish, *The Physical Principles of Magnetism* (IEEE, New York, 1980).

[33] T. Chatterji, *Neutron Scattering from Magnetic Materials*, edited by T. Chatterji (Elsevier, New York, 2005).

[34] T. Moriya, Prog. Theor. Phys. **28**, 371 (1962).

[35] N. Noginova, T. Weaver, M. King, A. Bourlinos, E. Giannelis, and V. Atsarkin, J. Phys.: Condens. Matter **19**, 076210 (2007).

[36] N. Noginova, T. Weaver, A. Andreyev, A. Radocea, and V. Atsarkin, J. Phys.: Condens. Matter **21**, 255301 (2009).

[37] M. Noginov, N. Noginova, O. Amponsah, R. Bah, R. Rakhimov, and V. Atsarkin, J. Magn. Magn. Mater. **320**, 2228 (2008).

[38] M. Fittipaldi, C. Innocenti, P. Ceci, C. Sangregorio, L. Castelli, L. Sorace, and D. Gatteschi, Phys. Rev. B **83**, 104409 (2011).